

引用格式:李文婧,吴南,匡增桂,等. 2026. 海底滑坡顶界面地貌形态对浊流的影响机制[J]. 沉积学报, 44(3): 977-993.

LI WenJing, WU Nan, KUANG ZengGui, et al. 2026. Top Surface Geomorphology of Submarine Landslides and Its Impact on Turbidity Currents[J]. Acta Sedimentologica Sinica, 44(3): 977-993.

DOI: 10.14027/j.issn.1000-0550.2024.105

CSTR: 32268.14/j.cjxb.62-1038.2024.105

海底滑坡顶界面地貌形态对浊流的影响机制

李文婧¹, 吴南¹, 匡增桂², 任金锋², 王毕文¹, 韩政豪¹, 陈万利³

1. 同济大学海洋地质全国重点实验室, 上海 200092

2. 广州海洋地质调查局, 广州 510075

3. 中国科学院深海科学与工程研究所, 海南三亚 572000

摘要 【目的】大型海底滑坡的失稳过程可导致数千平方千米的海底发生变形和破坏, 搬运数百—数千立方千米海底沉积物。这一过程极大地重塑了陆架—陆坡区的海底地形地貌, 并对后续的海底沉积过程产生深远影响。【方法】通过多波束水深数据和地震反射数据定性描述不同大型海底滑坡的顶界面形态特征, 以及定量刻画海底滑坡顶界面的面积和体积等关键几何参数, 基于海底滑坡顶界面伴生地貌的规模, 形态特征和形成机制等因素, 将海底滑坡顶界面伴生地貌形态划分为头部排空区、内部断层体系伴生局部负向空间和内部块体伴生局部负向空间三类, 并分别探讨这三类负向空间对后续浊流体系的影响机制。【结果】首先, 海底滑坡头部排空区通常伴生数百至数千平方千米的负向空间, 在陆缘沉积物运输过程中发挥“漏斗”作用, 能够有效捕捉和汇集后续浊流, 同时提高砾石、粗砂等粗粒碎屑沉积物的运输效率。其次, 海底滑坡内部断层体系伴生的条带状负向空间与海底滑坡内部变形块体伴生的不规则负向空间能够调控后续浊流体系的沉积动力过程, 例如约束浊流流向、增强浊流侵蚀强度以及迫使浊流水道决口等。最后, 大型海底滑坡顶界面伴生负向空间可能产生协同效应, 在数百万年的时间尺度内影响沉积盆地的充填演化过程和盆地沉积中心的分布位置。【结论】通过调研海底滑坡顶界面不同地貌形态及其对后续浊流沉积动力过程的控制作用, 可为厘清陆缘沉积物的运输过程、查明深海沉积盆地富砂储层的分布, 以及预测灾害性浊流的发育范围等提供关键的地质信息。

关键词 海底滑坡; 滑坡顶界面地貌特征; 海底浊流

第一作者 李文婧, 女, 2001年出生, 硕士研究生, 海底滑坡与浊流体系共生关系研究, E-mail: liwj1820@tongji.edu.cn

通信作者 吴南, 男, 副教授, 深海沉积学与地震/测井数据解释, E-mail: nanwu@tongji.edu.cn

中图分类号: P737.2 **文献标志码**: A **文章编号**: 1000-0550(2026)03-0977-17

0 引言

海底滑坡(submarine landslide)广泛存在于各个大陆边缘地区, 其失稳滑动过程具有极强的侵蚀性, 可以将大量陆源沉积物、有机碳和营养物质从大陆边缘输送至深海地区, 是洋陆沉积物输送的重要过程, 也是一种破坏性极大的海洋地质灾害(Nardin *et al.*, 1979; Nemeč, 1990; 吴时国, 2009; 王大伟等, 2011; 李伟, 2013; 孙启良等, 2021; 潘晓仪等, 2023)。大型海底滑坡的展布面积可达数千—上万平方米, 破坏搬运的沉积物体积可达数百—上千立方千

米(如 Storegga 滑坡、Mafia 滑坡、Gorgon 滑坡等; 表1)。依据海底滑坡的三维空间展布形态以及内部破坏应力性质, 海底滑坡通常被三分为头部拉张应力区(Extensional Domain), 体部过渡区(Translational Domain)和末端挤压应力区(Compressional Domain)(图1; Bull *et al.*, 2009)。海底滑坡通常发育平直且连续的底部界面(底部剪切面)和起伏不定的顶部界面, 在海底滑坡内部, 不同区域发育多种可指示滑坡运动过程的沉积构造类型, 如头部拉张断层系统、内部剪切应力条带、底部逃逸块体伴生的擦痕、滑坡末端挤压脊和逆冲断层系统等(图1)。大型海底滑坡

收稿日期: 2024-08-29; 修回日期: 2024-09-23; 录用日期: 2024-11-12; 网络出版日期: 2024-11-12

基金项目: 国家重点研发计划(2021YFC2800901); 中央高校基本科研业务费专项资金(22120240017); 海洋地质全国重点实验室探索课题(MGZ202303)

表1 大型海底滑坡统计表
Table 1 Statistics from large submarine landslides

序号	滑坡名称	发育地区	展布面积/km ²	体积/km ³	文献
1	The Sahara Slide	非洲西部陆缘	48 000	600	Georgiopoulou <i>et al.</i> , 2010; Li <i>et al.</i> , 2017
2	The Storegga Slide	挪威西北陆缘	35 000	3 500	Bondevik <i>et al.</i> , 2005; Hafliðason <i>et al.</i> , 2005
3	白云滑坡	中国南海珠江口盆地	13 000	1 035	Li <i>et al.</i> , 2014; Sun <i>et al.</i> , 2018a
4	The Mafia mega-slide	坦桑尼亚索马里盆地	11 600	2 500	Stagna <i>et al.</i> , 2023
5	The Ruatoria Debris Avalanche Deposit	新西兰北岛西北陆缘	7 000	3 100	Collot <i>et al.</i> , 2001; Moore <i>et al.</i> , 2023
6	The Brunei Slide	中国南海婆罗洲西北陆缘	5 500	6 500	Gee <i>et al.</i> , 2007
7	The Gorgon Slide	澳大利亚西北陆缘	1 760	500	Nugraha <i>et al.</i> , 2020a; Nugraha <i>et al.</i> , 2022

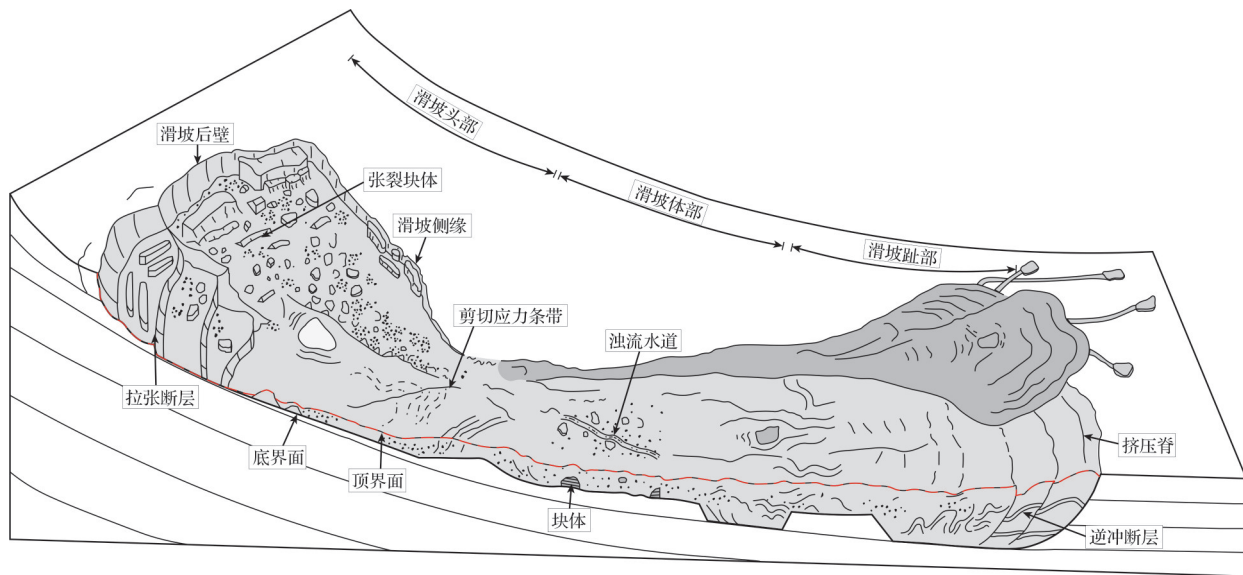


图1 海底滑坡典型三维空间展布形态模式图(据 Bull *et al.*, 2009 修改)

Fig.1 Three-dimensional (3D) distribution model of submarine landslides (modified from Bull *et al.*, 2009)

的失稳滑动过程可剧烈破坏海底地形地貌,其顶部界面在海底形成面积达数百至数千平方千米,体积达数十至数百立方千米的大型负向空间(图2;孙运宝等, 2008; Moscardelli *et al.*, 2008; Williams, 2016; Sun *et al.*, 2018b)。海底滑坡内部断层体系造成顶界面发育一系列数十至数百米高,数千米长的脊状正向地形和伴生的条带状负向空间(Bull *et al.*, 2009; 王大伟等, 2009; 陈珊珊等, 2012; 任金锋等, 2021), 内部变形块体亦在顶界面伴生数十米高,数百米宽的不规则盆地状负向空间(图2; Kneller *et al.*, 2016; Ward *et al.*, 2018; Steventon *et al.*, 2019)。海底滑坡顶界面上复杂的负向空间不仅可以充当汇集浊流沉积的可容空间,还能使得后续浊流、底流与其他海洋沉积过程的搬运机制和搬运路径发生转变,进而影响沉积物的分布范围和沉积盆地的演化历史(Ortiz-Karpf *et al.*, 2015; Nwoko *et al.*, 2020; Wu *et al.*, 2024)。

本文调研了通过三维地震数据研究大型海底滑坡的案例,关注滑坡顶界面的地震地貌形态,基于规模、形态、成因等因素对其伴生的负向空间类型进行分类;在此基础上,探讨滑坡顶界面不同负向空间类型对后续浊流体系的控制机制,旨在为理解海底滑坡顶界面在调控大陆边缘“源—汇”体系、深海沉积盆地的充填演化过程以及海洋油气成藏中的重要作用提供参考。

1 海底滑坡顶界面的地震地貌特征

海底滑坡顶界面是滑坡在失稳堆积后,其顶部与上覆未扰动沉积物之间的界面。然而,在有后续流体经过的区域,顶界面可能为流体下切侵蚀形成的沟槽,或滑坡顶部与上覆流体改造沉积物的界面。海底滑坡顶界面在地震剖面上通常具有中等—较强的振幅、不规则的形态、可大范围连续追踪等特征,还可能留存浊流水道侵蚀不整合面等结构。海底滑

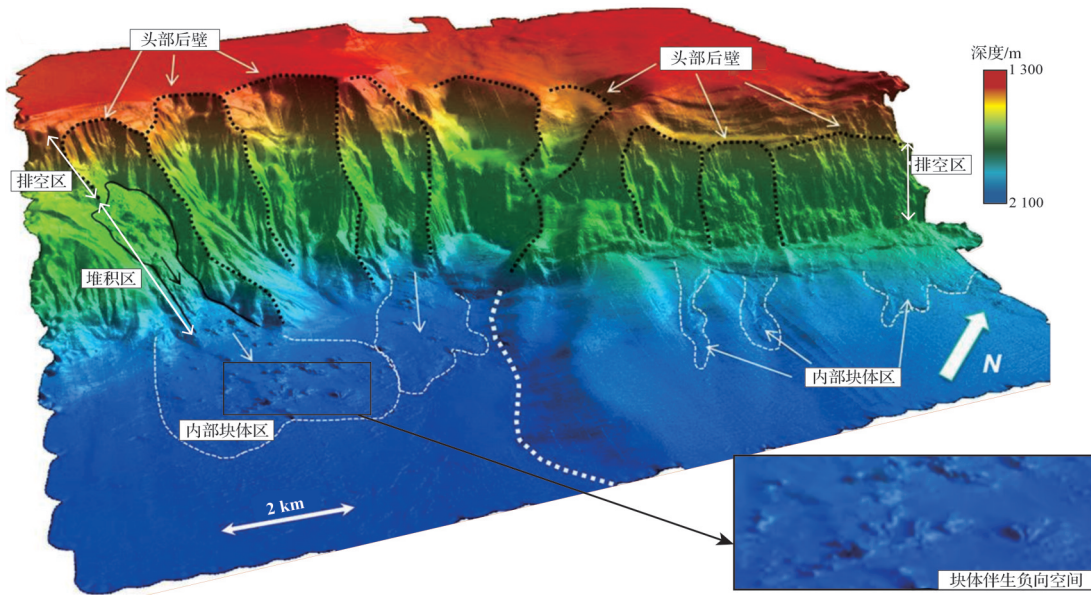


图2 墨西哥湾 Sigsbee 悬崖大型海底滑坡地形地貌图(据 Williams, 2016 修改)

Fig.2 Topographic map of large-scale submarine landslides on the Sigsbee cliff, gulf of Mexico (modified from Williams, 2016)

坡失稳堆积后,其顶界面会在海底形成一系列规模、形态各异的负向空间 (Armitage *et al.*, 2009; Olafiranye *et al.*, 2013; Ortiz-Karpf *et al.*, 2018; Nwoko *et al.*, 2020)。本文依据海底滑坡顶界面伴生的负向空间的位置、平面形态、规模与成因,将其分为三种不同类型(表2)。

1.1 海底滑坡头部排空区

海底滑坡失稳过程侵蚀破坏能力极强,在头部区域形成一个数百至上千平方千米的大规模负向空间。该负向空间位于海底滑坡头部后壁与堆积区之间,形成四周高、中间低的“地堑”式平面形态(图2; Williams, 2016)。基于此负向空间的空间形态、相对海底滑坡头部后壁的发育位置,前人将其定义为海底滑坡头部排空区 (Evacuation Zone; Nugraha *et al.*, 2020; Nugraha *et al.*, 2020a)。例如,伴生在澳大利亚

西北陆缘的 Gorgon 滑坡的巨大排空区长约 35 km, 宽约 18 km, 展布面积约 500 km², 体积约 46 km³ (图3; Nugraha *et al.*, 2022)。平面上,该排空区在现代海底形成由多个弓形后壁断层(高约 100~350 m)和侧壁断层(高约 90 m)所限定的“铲状”侵蚀凹陷。在沿滑动方向的地震剖面上,该排空区以头部后壁和趾部堆积区为界,形成上宽下窄的楔形负向空间(图3)。

1.2 海底滑坡内部断层体系伴生局部负向空间

海底滑坡的失稳滑动过程中存在拉张变形、挤压变形、剪切变形等多种破坏过程 (Martinsen and Bakken, 1990; Bull *et al.*, 2009)。不同变形过程在海底滑坡内部不同部位形成一系列独特的断层配套样式 (Bull *et al.*, 2009; 何叶和钟广法, 2015), 如拉张变形通常集中在海底滑坡的头部区域, 而挤压变形主要发育于趾部区域, 剪切变形则主要集中在体部区

表2 海底滑坡顶界面伴生的负向空间类型

Table 2 Types of negative space associated with the top surface of a submarine landslide

类型	发育位置	形态	规模	成因	实例
排空区	滑坡头部	地堑式凹陷	展布面积数百至上千平方千米	海底滑坡物源区沉积物被破坏搬运	澳大利亚西北陆缘 Gorgon 滑坡 (Nugraha <i>et al.</i> , 2022)、巴西东南部沿海 Santos 盆地北部大规模海底滑坡 (Buso <i>et al.</i> , 2024) 等
断层体系伴生局部负向空间	滑坡头部、趾部及边界处	相互平行展布的条带状凹陷	长数千—数千米、宽数百—数千米、深数十米, 展布面积数千至上万平方米	海底滑坡内部拉张或挤压破坏过程	挪威西北陆缘 Storegga 滑坡头部区域 (Micallief <i>et al.</i> , 2016)、印尼望加锡海峡南侧 Haya 滑坡 (Nugraha <i>et al.</i> , 2020b) 等
变形块体伴生局部负向空间	滑坡体部	半封闭—封闭的似碗状凹陷	长数十—数百米、宽数百米、深数米—数十米; 闭合面积数千至上万平方米	滑坡内部发育变形块体	新西兰 Taranaki 盆地海底滑坡 (Bull <i>et al.</i> , 2020)、巴西东南部 Espírito Santo 盆地海底滑坡 (Ward <i>et al.</i> , 2018) 等

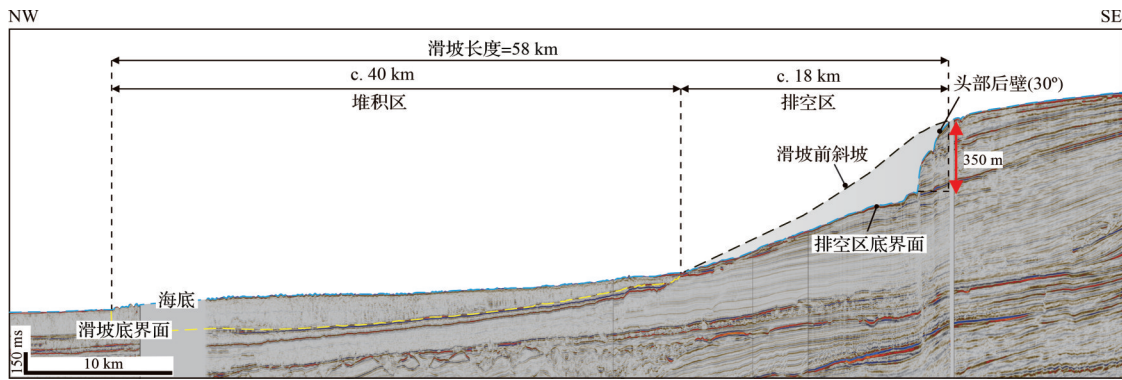


图3 澳大利亚西北缘 Gorgon 滑坡地震剖面图 (据 Nugraha *et al.*, 2022 修改)

Fig.3 Seismic profile of the Gorgon slide on the northwest margin of Australia (modified from Nugraha *et al.*, 2022)

域,表现为失稳沉积物之间的相对剪切滑动。

1.2.1 拉张应力正断层

拉张变形过程主要存在于海底滑坡的初始阶段,在海底滑坡头部区域形成一系列正断层和铲状

断层组合形式。这些正断层在平面上呈现上凹状弧形形态,在剖面上则表现为后退式和阶梯状组合形式(图4; Bull *et al.*, 2009; Sawyer *et al.*, 2009)。以挪威西北陆缘 Storegga 滑坡为例,受到正断层影响,该

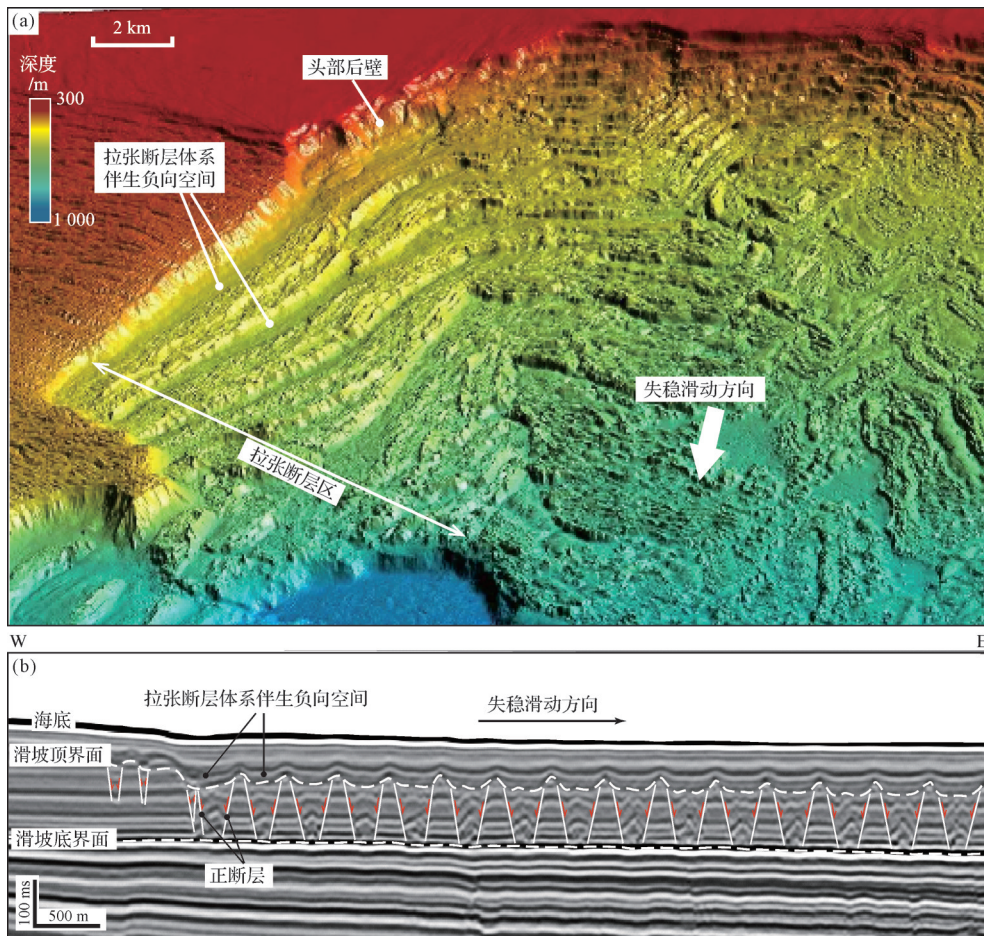


图4 (a) 挪威西北陆缘 Storegga 滑坡头部拉张断层体系地形地貌图 (据 Micallef *et al.*, 2016 修改);

(b) 澳大利亚西北陆缘海底滑坡头部拉张断层体系地震剖面图

Fig.4 (a) Topographic map of the headwall tension fault system of the Storegga slide, northwest continental margin of Norway (modified from Micallef *et al.*, 2016); (b) seismic profile of the head tension fault system of a submarine landslide along the northwest continental margin of Australia

海底滑坡顶部发育一系列条带状、相互平行展布的负向空间(图4a; Micallef *et al.*, 2016)。这些负向空间周缘被正断层下盘限定,长轴平行于正断层走向,其长度介于10~20 km,宽度介于1~2 km,长宽比介于10~20,面积约20 km²。在地震剖面中(图4b),正断层伴生负向空间呈规则且宽缓的“U”型凹陷形态,深度约50 m,相邻凹陷被一组在顶界面相交的正断层分隔,单一凹陷相对孤立,凹陷内沉积物呈平行或近平行充填,两端同相轴呈上超或削截终止于正断层处,厚度由凹陷中间往两侧减薄。

1.2.2 挤压应力逆断层

挤压变形过程多存在于海底滑坡失稳滑动末期,受到挤压变形影响,海底滑坡趾部区域多见逆断

层和逆冲断层体系的组合形式(Frey-Martínez *et al.*, 2006; Moscardelli *et al.*, 2006; Scarselli *et al.*, 2013)。这些逆断层在平面上呈现一系列相互平行、上凹状的弧形曲线,在剖面中呈现一系列叠瓦状排列组合形式(图5; Moernaut *et al.*, 2011; Ortiz-Karppf *et al.*, 2018; Nugraha *et al.*, 2020b)。以印尼望加锡海峡南侧 Haya 滑坡为例,受到挤压应力逆断层影响,该海底滑坡顶部发育一系列狭窄条带状、相互平行展布的负向空间(图5a; Nugraha *et al.*, 2020b)。这些负向空间被逆断层形成的挤压脊所限定,长轴走向垂直于滑坡失稳滑动的方向,长度介于2.5~30.0 km,宽度介于0.1~2.0 km,长宽比变化范围较大(5~30),面积介于2.5~10.0 km²。在地震剖面中(图5b),逆断层伴生

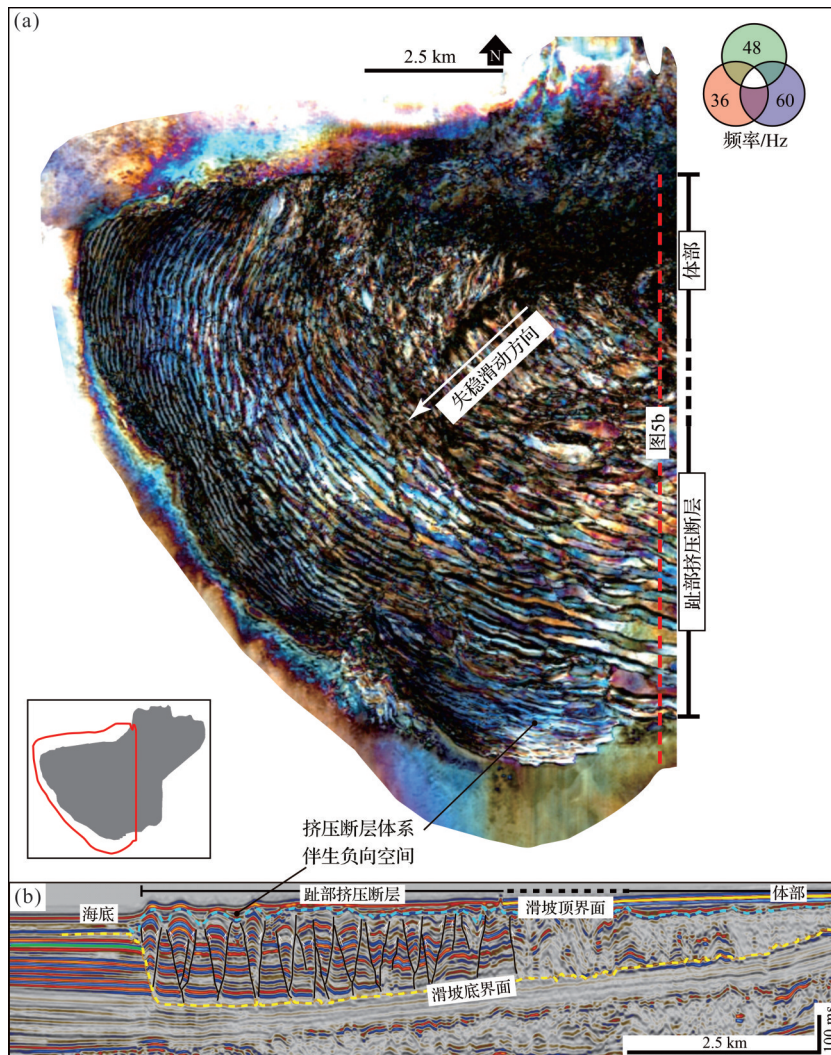


图5 (a)印尼望加锡海峡南侧 Haya 滑坡趾部挤压断层体系顶界面地震频率属性图;
(b) Haya 滑坡趾部挤压断层体系地震剖面图(据 Nugraha *et al.*, 2020b 修改)

Fig.5 (a) Seismic frequency attribute map of the top surface of toe compression faults from the Haya slide on southern Makassar Strait, Indonesia; (b) seismic profile of the toe compression faults of the Haya slide (modified from Nugraha *et al.*, 2020b)

的负向空间呈不规则碟状凹陷形态,深度约50 m,相邻凹陷被逆断层上盘所形成的背斜控制,单一凹陷相对孤立,凹陷内沉积物呈平行或近平行充填,同相轴向背斜两翼上超或削截。

1.2.3 剪切应力走滑断层

剪切变形是海底滑坡内部最为常见的破坏过程,是内部沉积物在剪切应力的作用下发生相对运动并快速变形的破坏过程(Steventon *et al.*, 2019; Nugraha *et al.*, 2020a; Abu *et al.*, 2022)。海底滑坡内部沉积物受到不均匀剪切应力时,失稳滑动速度会产生差异,在顶界面产生脊状的剪切应力条带。剪切应力条带的长轴展布方向与滑坡失稳滑动方向平行或亚平行,在平面上呈长条状或蛇曲状的线型构造(图6a)。以澳大利亚西北缘Gorgon滑坡为例,剪切应力条带长度超过10 km,宽度为200 m,垂直高度为20 m,平面上呈蛇曲状,其伴生的负向空间呈条带状,长度与剪切应力条带相近(图6a; Nugraha *et al.*, 2020a)。在地震剖面中(图6b),针尖状向上隆起的剪切应力条带将海底滑坡顶界面分为左右不同的地貌单元,海底滑坡块体或碎屑沉积物与剪切应力条带在顶界面上共同限定了一个宽度约2 km,深度约20 m的盆状负向空间。

1.3 海底滑坡内部变形块体伴生局部负向空间

海底滑坡失稳滑动过程中,内部块体受到破坏应力影响发生旋转或变形程度加剧,导致块体具有不规则和锯齿状的几何外形(Alves, 2015; Amaechi *et al.*, 2023)。这些块体在平面上一般呈无序分布,在滑坡顶界面形成正向“锥型”或“地台”型地貌(图1、

图7a),在剖面中块体向上倾斜或隆起形成地形高点(图7b)。以新西兰Taranaki盆地海底滑坡内部块体区为例,该区域块体高度为150~250 m,宽度为0.5~2.0 km。平面上(图7a),块体间发育多个半闭合或闭合的、不规则的似盆地状负向空间。在地震剖面中(图7b),块体伴生负向空间呈独立或相互连通的似碗状凹陷形态,宽度介于0.1~2.0 km,深度介于20~100 m,宽深比介于10~20,两侧被向上凸起的块体顶部边缘所限定,凹陷内沉积物呈平行或近平行充填,厚度从中间向块体两侧减薄。

2 海底滑坡顶界面对后续浊流体系的控制作用

海底滑坡顶界面复杂的地形地貌改变了海底坡度,形成一系列局部的正向地形和不同形态、规模的负向空间,对后续浊流、底流、海底滑坡等沉积过程产生深远影响。本节将针对海底滑坡顶界面不同地貌形态对后续浊流体系的调节和控制作用展开讨论。

2.1 海底滑坡头部排空区对后续浊流体系的汇聚作用

海底滑坡头部的大规模排空区增大了海底陆坡上部的沉积物可容空间,便于汇聚和容纳更多浊流及其伴生扇体携带的沉积物。以发育在巴西东南缘Santos盆地大型海底滑坡为例(图8; Buso *et al.*, 2024),该滑坡头部发育后壁倾角约20°,高约250 m,宽800 m、展布面积约8 km²的排空区。排空区内部

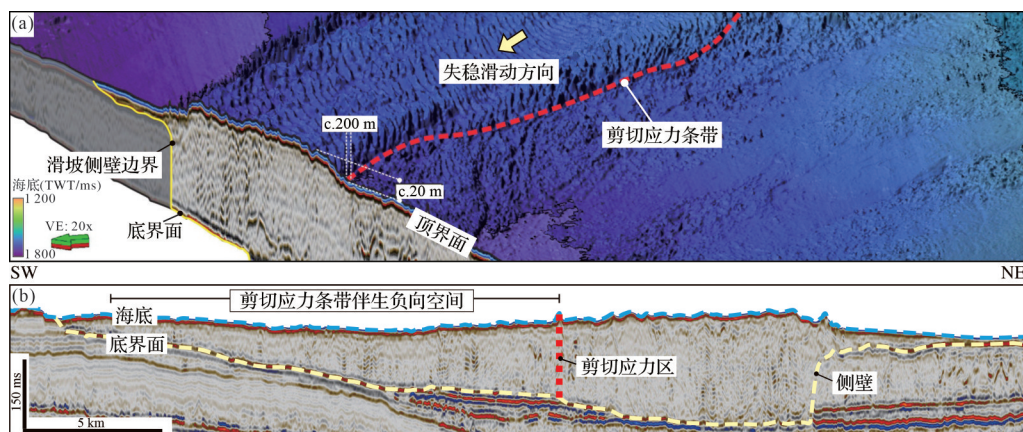


图6 澳大利亚西北缘Gorgon滑坡剪切应力条带(a)地形地貌图;(b)地震剖面图
(据Nugraha *et al.*, 2020a 修改)

Fig.6 (a) Topographic map of longitudinal shear zone of the Gorgon landslide, northwest margin of Australia;
(b) seismic profile of the longitudinal shear zone of the Gorgon landslide (modified from Nugraha *et al.*, 2020a)

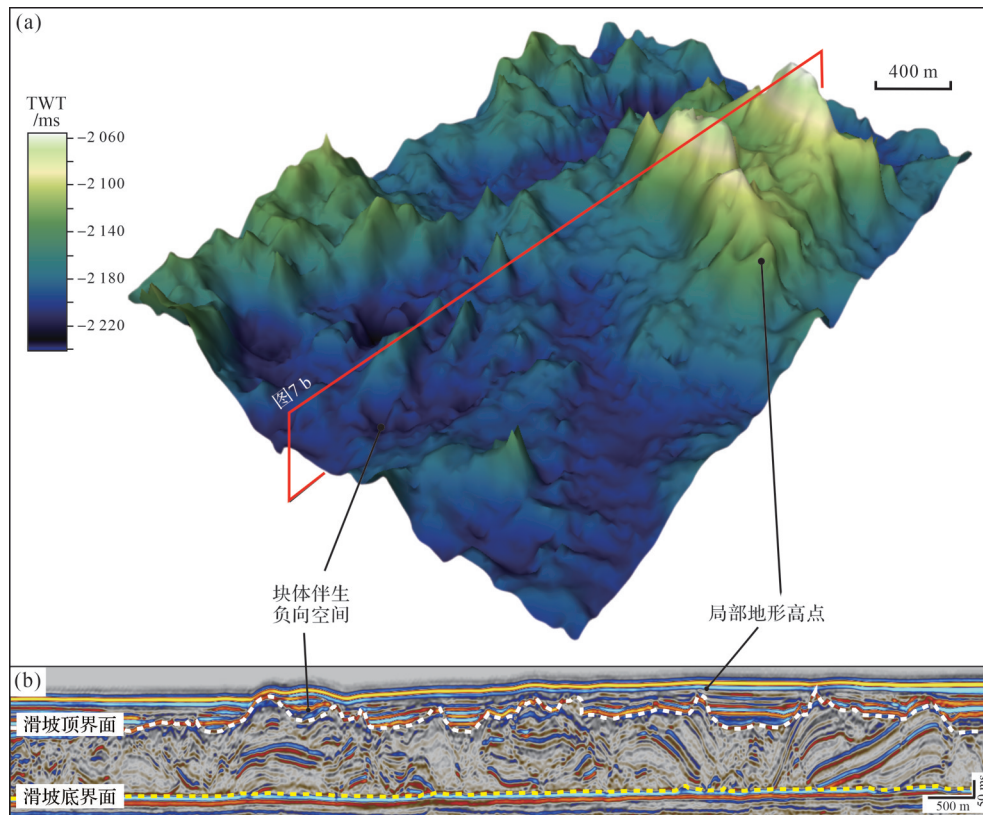


图7 新西兰Taranaki盆地海底滑坡块体区(a)三维地形地貌图;(b)新西兰Taranaki盆地海底滑坡块体区剖面图

Fig.7 (a) 3D topographic map of the blocky area of the submarine landslide in Taranaki Basin, New Zealand;
(b) seismic profile of the blocky area of the submarine landslide from (a)

发育多期纵向叠置的S型前积反射结构,在地震剖面中形成壮观的前积反射复合体(图8b)。这套前积层复合体发育了进积型准层序样式,并呈现下降型迁移轨迹。这些特征表明,海底滑坡发生后,陆架沉积物在滑坡头部排空区内迅速向盆地(深海)推进,排空区很快被陆源沉积物充填,从而增加了在深海形成厚层砂体的可能性(Henriksen *et al.*, 2011)。然而,这一现象通常发育于海平面快速下降时期(丛富云和徐尚, 2017)。与此形成对比的是,进积型准层序组的上部发育了一套呈现上升型迁移轨迹的加积型准层序组,表明在海底滑坡头部排空区周缘,沉积物输入速率相对稳定,未出现快速海退沉积环境(图8b)。因此,在与陆源河流相连的沉积盆地系统内,海底滑坡头部巨大的排空区可以在海平面稳定的条件下,促使沉积盆地经历类似强制海退的过程。这一过程增加了陆源泥沙和有机质等在陆坡沉积埋藏的比例,不仅为近岸油气藏提供了丰富的物源和良好的储集条件,还与后续发育的底积层和顶积层内富有机质细粒沉积物共同作用,形成深水油气圈闭。

此外,海底滑坡头部排空区可作为大陆斜坡“源—汇”系统主要沉积物传送带,增加后续浊流水道的沉积物搬运量。在坦桑尼亚索马里盆地的Mafia滑坡及其区域的浊流水道系统中,海底滑坡发生前,陆坡区发育了多期相互平行展布的浊流水道体系(图9a; Stagna *et al.*, 2023)。这些水道彼此平行排列,且每一期的浊流水道在横向上相互独立,因此各水道所携带的砂体互不连通,空间上呈现出孤立发育的特征。Mafia海底滑坡的失稳滑动导致陆坡区大量沉积物遭到破坏,并随着滑坡的移动被搬运至深海区域,这一过程在陆坡处形成了巨大的排空区(图9b)。Mafia海底滑坡伴生的排空区促使原本孤立发育的浊流水道体系迅速汇聚,在排空区内形成了更宽广、下切深度更大的新浊流水道体系(图9c)。同时,新生成的浊流水道体系中粗粒碎屑沉积的比例显著增加,砂体由原先的孤立分布转变为大规模的连片状分布。这一结果表明滑坡头部区域由于排空区的存在,铲状的负向空间具有“漏斗效应”(图9b),可以汇集浊流并扩大水道体系的规模,促使更多的水道浊积砂体和陆源粗粒碎屑沉

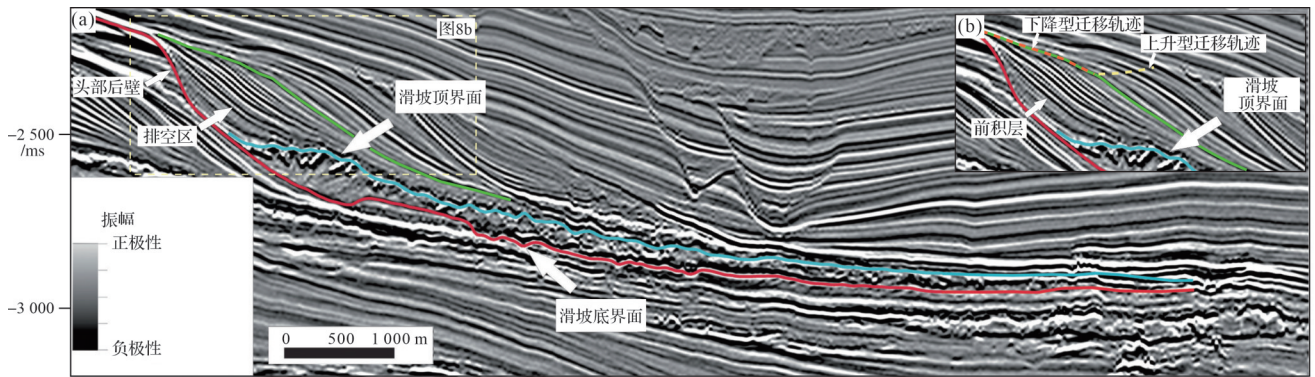


图8 (a)巴西东南部沿海 Santos 盆地北部海底滑坡排空区为后续浊流沉积提供大型可容空间;(b)排空区提高了后续浊流沉积的搬运速率,前积层复合体发育典型的下降型迁移轨迹(据 Buso *et al.*, 2024 修改)

Fig.8 (a) Evacuation zone of a submarine landslide in the northern Santos Basin, southeast Brazil, which provides a large accommodation for subsequent turbidity sediment; (b) evacuation zone increases the transport rate of subsequent turbidity sediment, and the fore-prograde complex develops a typical descending migration trajectory (modified from Buso *et al.*, 2024)

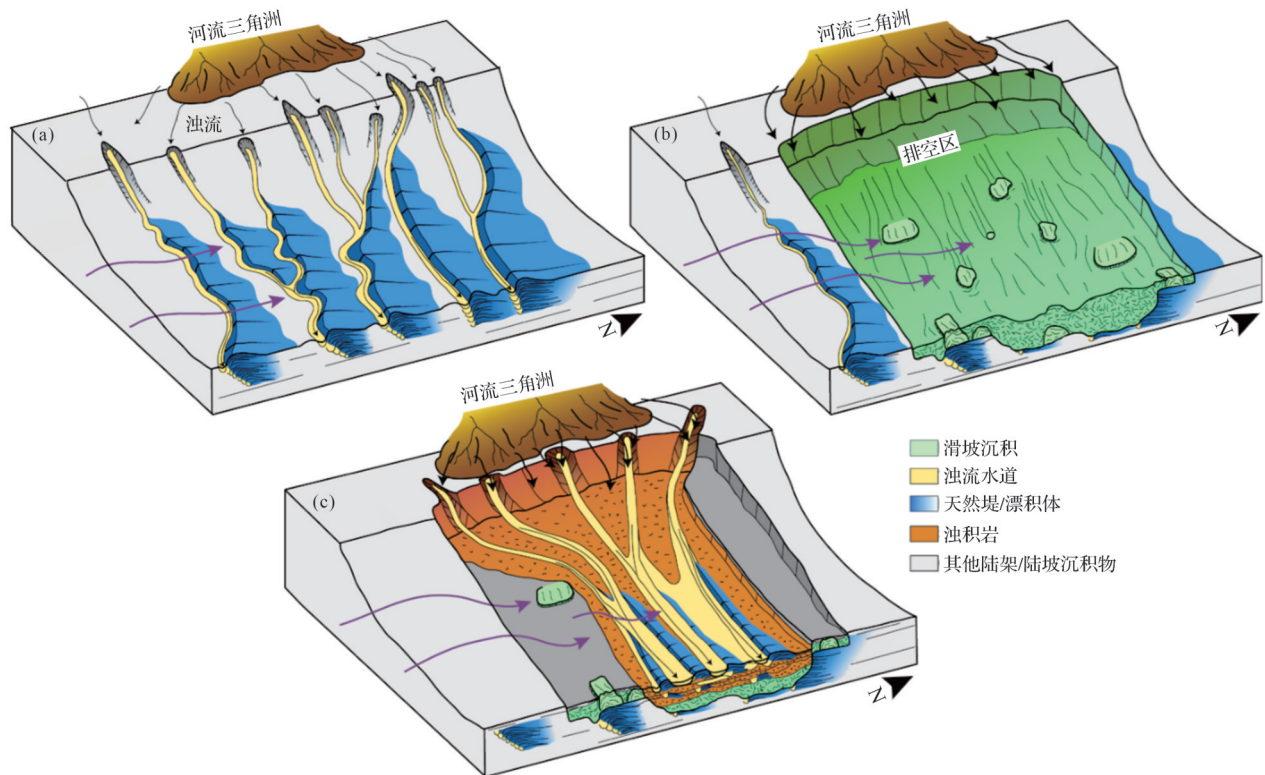


图9 坦桑尼亚索马里盆地 Mafia 滑坡排空区对浊流水道体系的控制作用示意图(据 Stagna *et al.*, 2023 修改)

(a)海底滑坡发生前的浊流水道体系;(b)滑坡失稳形成头部排空区;(c)滑坡发生后的浊流水道体系

Fig.9 Schematic diagram of the Mafia Slide evacuation zone controlling turbidity channel system in the Somalia Basin, Tanzania (modified from Stagna *et al.*, 2023)

(a) pre-slide turbidity channel system; (b) landslide failure forming evacuation zone; (c) post-slide turbidity channel system

积物进入滑坡并滞留在滑坡近端区域(图9c)。从斜坡沉积系统考虑,滑坡排空区可以促进富砂相沉积环境的形成,使得滑坡头部区域成为有利的砂体和陆源有机质富集区,这对深水盆地油气储层的预测

具有重要意义。

海底滑坡头部排空区还可以作为浊流的优先通道,汇聚浊流和浊流水道从而增强浊流整体的动能和侵蚀能力,促进水道或峡谷的发育过程。以巴西

东南部 Espírito Santo 盆地上新世—第四纪的海底滑坡与水道体系为例,浊流水道和无限限制浊流在通过海底滑坡头部排空区后发生了合并,形成宽度、深度、汇水面积都明显增加的浊流水道体系(图 10; Qin *et al.*, 2017)。该区域海底滑坡头部排空区与周围海底高差约为 200 m,是一个天然的地形低点,因此后续水道和浊流会优先进入滑坡区域(图 10a),同时经过滑坡头部的汇集和重力势能的转换(图 10b),以及侧壁的遮挡作用(图 10c),水道内浊流的流量和侵蚀能力增强,在滑坡内形成更大规模的水道体系(图 10d)。海底滑坡头部排空区发生的汇水效应,说明排空区的大规模负向空间能够为浊流赋能,促进海底水道和峡谷的形成,增强陆缘“源—汇”系统的搬运效率。

2.2 滑坡内部断层体系伴生负向空间为后续浊流长距离搬运赋能

海底滑坡头部一系列拉张正断层的起伏地形及其伴生的负向空间可影响后续洋流(包括底流、陆架瀑布流和其他海底洋流)流动过程,造成洋流向浊流转换。以澳大利亚东南部 Gippsland 盆地陆架区域海底滑坡为例,该盆地的陆架区发育季节性沿外陆架流动的陆架瀑布流(Dense Shelf Water

Cascade, DSWC)(图 11a; Wu *et al.*, 2024)。陆架瀑布流底部携带大量悬浮状的沉积物水团,在流入海底滑坡区之前,该水团保持相对稳定的状态。陆架瀑布流经过海底滑坡头部断层时发生下沉(图 11c, d),陆架瀑布流平衡状态被破坏。滑坡头部断层的高差(40~70 m)所产生的重力势能,促进了陆架瀑布流底部水团及沉积物的动能和流速的增加。流速的提升引起了水团周围沉积物的扰动,进一步使周围沉积物再悬浮并增加了水团内沉积物的密度(图 11d),最终形成了垂直于陆坡方向的持续稳定的浊流体系。这一过程表明海底滑坡头部断层体系的存在为洋流向浊流的转化提供了动力,使该地区的浊流可以长时间、稳定地进行沉积物搬运和侵蚀作用,为海底峡谷的孕育提供了有利条件,构成从浅海向深海环境搬运营养物质、有机碳、粗粒碎屑等沉积物的优先通道,对生物地球化学循环和碳封存具有重要影响。

海底滑坡失稳滑动遵循后退式(retrogressive)演化模式,因此滑坡头部及其邻近区常发育一系列平面呈新月状排列(图 12a),剖面呈阶梯状的正断层体系(图 12b; Sawyer *et al.*, 2009)。接连分布的正断层在海底滑坡内部形成一系列断崖状的负向海底地

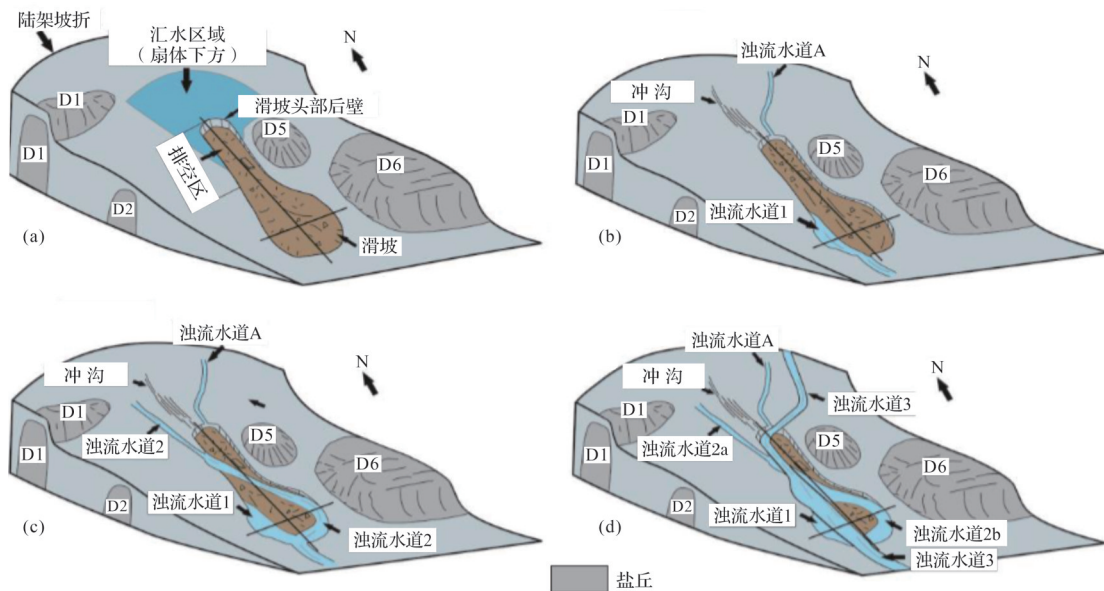


图 10 巴西东南部 Espírito Santo 盆地海底滑坡排空区对浊流的汇集作用(据 Qin *et al.*, 2017 修改)

(a)排空区负向地形使其成为优先汇水区;(b)排空区汇集后续无限制浊流和浊流水道 A;(c)滑坡侧壁断层对浊流水道 1, 2 起遮挡作用;(d)在滑坡中形成规模更大的浊流水道 3;D1, D2, D5, D6 为盐底辟

Fig.10 Pooling of turbidity currents in the submarine landslide evacuation zone of Espírito Santo Basin (SE Brazil) (modified from Qin *et al.*, 2017)

(a) the negative accommodation of the evacuation zone makes it a priority catchment area; (b) the evacuation zone catches subsequent unrestricted turbidity currents and turbidity channel A; (c) the sidewall fault of the landslide resisted turbidity channels 1 and 2; (d) formation of larger turbidity channel 3 in landslide scarp; D1, D2, D5, and D6 indicate salt diapirs

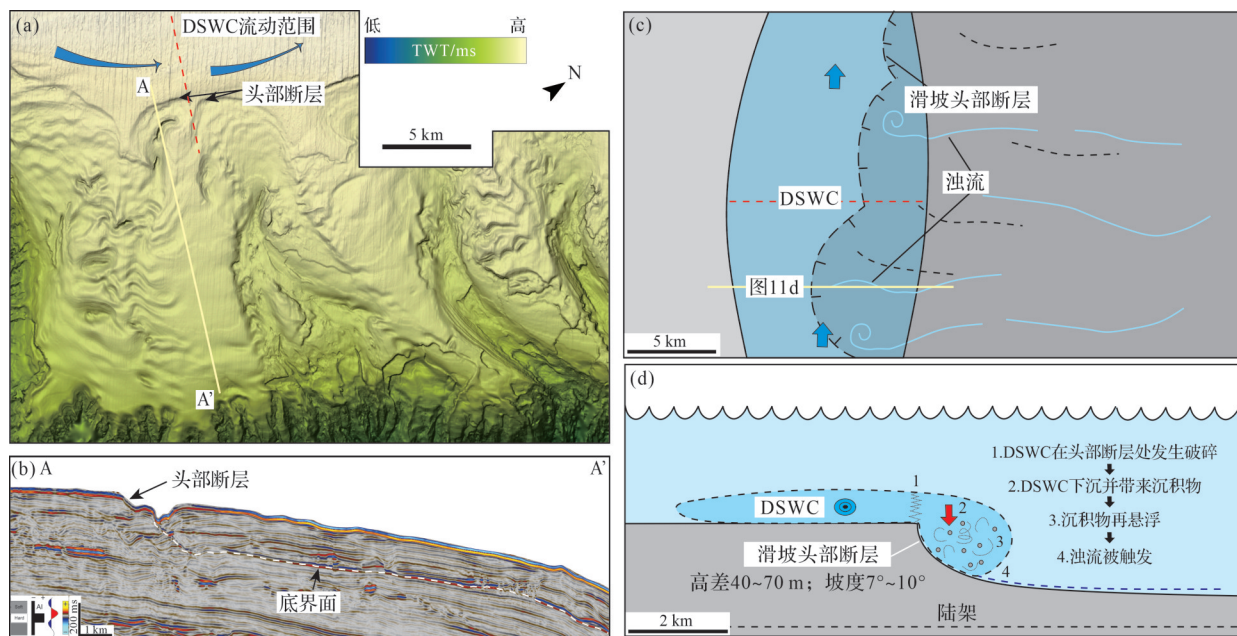


图11 (a)澳大利亚东南部 Gippsland盆地巴斯峡谷头部海底滑坡区;(b)海底滑坡头部断层在剖面上呈现大坡度陡坎;(c, d)陆架瀑布流(Dense Shelf Water Cascade, DSWC)与海底滑坡头部断层相互作用示意图
(据 Wu *et al.*, 2024 修改)

Fig.11 (a) Submarine landslides located at the head of Bass Canyon in the Gippsland Basin, southeast Australia; (b) the headwall fault manifests as a significant steep slope on the profile; (c, d) schematic diagram illustrating the interaction between Dense Shelf Water Cascade (DSWC) and the headwall fault of submarine landslide (modified from Wu *et al.*, 2024)

形,并随地势差异。后续浊流体系经过这些区域时,海底局部负向地形特征有助于增强浊流的侵蚀能力,进而促进形成更大规模的浊流水道(图12c),甚至演化为海底峡谷。例如,澳大利亚东南部 Otway 盆地陆坡区发育海底滑坡和峡谷共生沉积体系,该海域海底滑坡内部至少发育了五期头部断层(图12a),这些断层在剖面上伴生一系列局部错断(图12b),且错断的规模随着接近海底滑坡头部区域逐渐增大(Wu *et al.*, 2022)。同时,海底滑坡内部发育浊流水道(浊流水道1、2、3),这三期水道在经过一系列海底滑坡伴生台阶状头部断层体系(图12a,头部断层5、4、3、2、1)后逐渐汇集并演化成为下切深度更深、宽度更大的海底峡谷体系(图12c)。研究表明,海底滑坡头部及其邻区发育的多级头部断层可分别形成数十米的高差地形,这些呈阶梯状下降的地貌构型使得浊流水道内的流体发生连续的重力势能转换,从而显著增加流体的动能和侵蚀能力。同时,滑坡头部断层体系所伴生的负向空间受正断层断距的影响,中部地势较低,导致加速的浊流在断层中部汇集,最终演化成更大规模的海底水道。滑坡头部断层体系与浊流水道的相互作用

过程,不仅促进了海底水道和峡谷的发育演化,也有利于浅海沉积物向深海盆地进行长距离、高效的搬运。

2.3 滑坡内部块体伴生顶界面地貌形态控制浊流体系的搬运路径

海底滑坡内部块体与其伴生的局部负向空间在海底滑坡顶界面形成高一低一高的起伏地形,控制后续水道的流向。以新西兰西部深水 Taranaki 盆地海底滑坡为例(图13),水道在遇到块体时会发生分流(图13a),大部分流体偏转流入块体间的地势更低的区域(图13b),而被分流的另一侧水道则逐渐消失,证实了海底滑坡内部块体形成的局部地形高点会使后续水道发生分流和偏转,且地势更低的局部负向空间汇集、约束浊流的能力更强(Bull *et al.*, 2020)。此外,块体伴生局部负向空间的连通性也影响了后续水道的流向和沉积分布范围。以巴西东南部 Espírito Santo 盆地海底滑坡为例(图14),相对孤立的负向空间则可以作为后续浊流的天然沉积中心(图14b),而连通性较好的块体伴生局部负向空间可作为后续浊流的优先通道(图14c; Ward *et al.*, 2018)。最后,随着顶界面上的负向空间逐渐被充

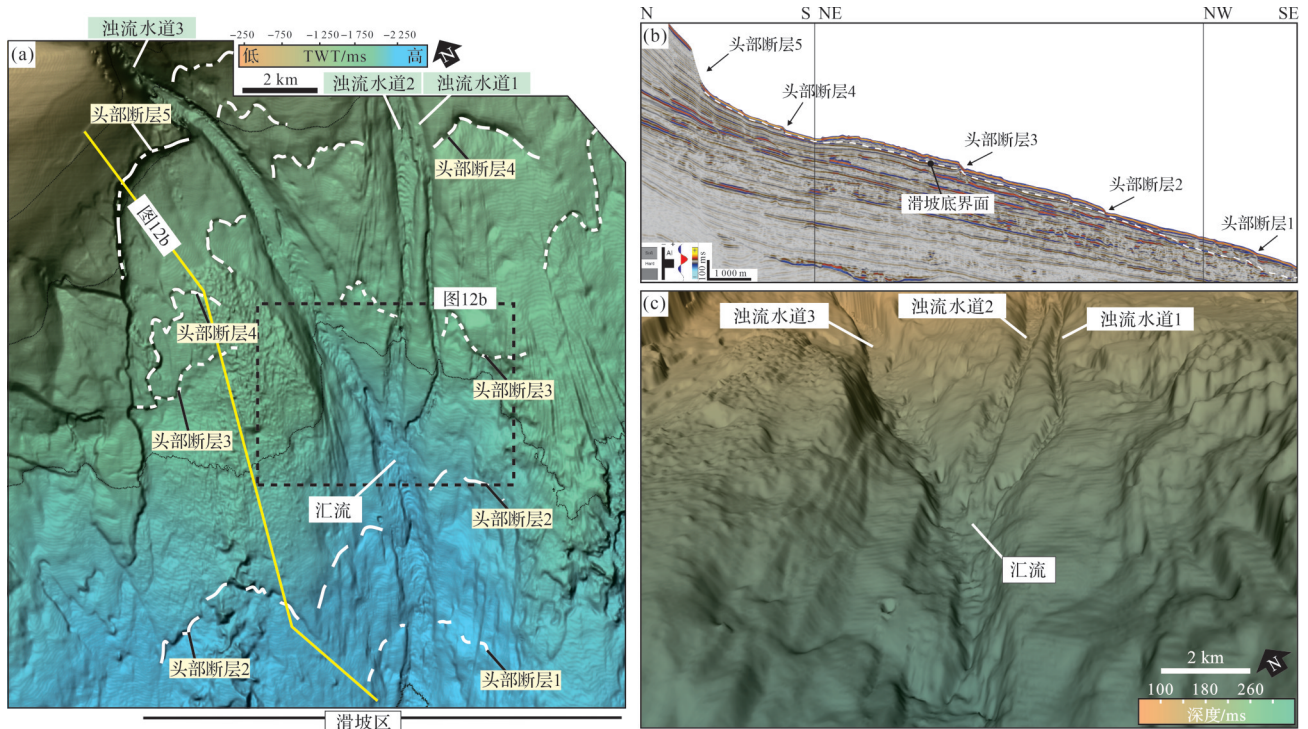


图 12 (a)澳大利亚东南部 Otway 盆地海底滑坡发育一系列台阶状头部断层(编号为 1~5);(b)海底滑坡头部断层在剖面上表现为多级阶梯状陡坎;(c)海底滑坡头部断层通过连续的地势差为浊流水道赋能,使浊流水道(编号为 1~3)汇流形成宽度、深度都明显增加的浊流水道体系(据 Wu *et al.*, 2022 修改)

Fig.12 (a) Series of step-shaped headwall faults (No. 1, 2, 3, 4 and 5) developed in submarine landslide in the Otway Basin, south-east Australia; (b) the headwall faults of the submarine landslide are characterized by multi-steps steep slope in cross-section; (c) the headwall faults of the submarine landslide empower the turbidity channel through continuous terrain declines; thus, the confluence of turbidity channels 1, 2, and 3 forms a turbidity channel system with significantly increased width and depth (modified from Wu *et al.*, 2022)

填,顶界面地貌形态对后续沉积物流体的约束作用会逐渐减弱,但滑坡块体与周围碎屑沉积以及上覆沉积物之间的岩性差异会产生不同程度的压实作用,导致滑块在掩埋后很长一段时间(>5 Ma)仍影响着后续海底地形的起伏和现代海底浊流水道体系的分布。因此,海底滑坡内部块体伴生顶界面地貌形态可以长时间地调控后续浊流的流向和沉积中心的位置,决定滑坡区水道体系的展布范围和搬运路径。

海底滑坡内部块体形成的顶界面地形高点和伴生的局部负向空间还会影响后续浊流水道决口位置和沉积物再分布范围。以哥伦比亚北部加勒比海 Magdalena 海底扇海底滑坡和水道体系为例(图 15),海底滑坡内部块体在顶界面形成地形高点(图 15a),增大了海底地形的坡度变化,为后续浊流水道天然堤沉积在块体侧缘发生滑塌提供了有利的预处理条件(图 15b),最终导致水道决口,形成决口扇(图 15c;

Ortiz-Karpf *et al.*, 2015)。在水道决口的初期,富泥质的天然堤沉积物率先进入块体伴生的局部负向空间(图 15b),随后,水道内的砂质浊流沉积沿决口进入天然堤滑塌形成的负向空间形成叶状复合体(图 15c)。滑坡顶界面地形对水道决口的控制,是浊流与块体区地形起伏相互作用的结果,决口沉积由泥向砂的演变可构成良好的油气生储条件,对海底斜坡油气勘探选区有重要意义。

2.4 滑坡顶界面地貌形态对沉积盆地演化过程的控制作用

海底滑坡的顶界面地貌形态不仅可以影响后续的浊流事件,还能从更长地质时间、更宏观空间尺度上调控后续沉积盆地充填演化历史。以安哥拉陆缘下刚果盆地内的海底滑坡为例,海底滑坡堆积被埋藏后,滑坡内部的断层体系与大型块体共同作用,在地震层单元 2(SU2)顶部形成了起伏高达 150 m 的背斜式地形高点,并在其周围产生了大规模的向斜

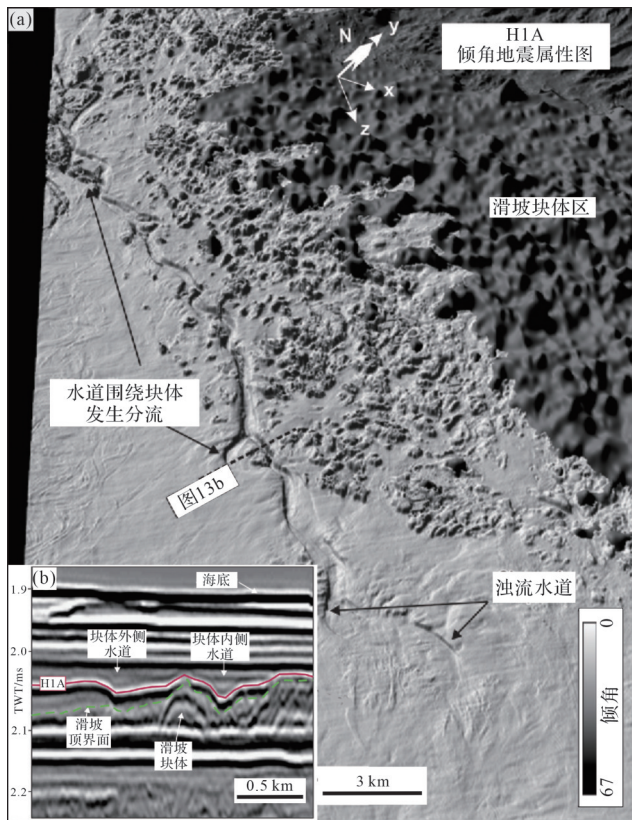


图13 (a)新西兰西部深水Taranaki盆地海底滑坡块体区中,浊流水道围绕块体发生分流;(b)浊流水道优先从块体地势较低的一侧流过(据Bull *et al.*, 2020修改)

Fig.13 (a) In the submarine landslide blocky area of the deep-water Taranaki Basin in western New Zealand, turbidity channels are bifurcate around the blocks; (b) the turbidity channel preferentially flows through the low-lying side of the block (modified from Bull *et al.*, 2020)

式负向空间(图16a,b),进而影响了后续浊流体系的沉积中心位置,并控制了整个研究区上新世—全新世地震层序单元3至单元5(SU3~SU5)的沉积厚度(图16a;Olafiranye *et al.*, 2013)。地震层序单元2顶部负向空间有效捕获了后续的砂质浊流沉积,进而在地震层序单元(SU3)中形成一系列近环形,面积16~20 km²,深120~150 m的沉积中心(图16c)。地震层序单元(SU3)中的沉积中心展布特征及沉积物的充填过程表明,海底滑坡顶界面所形成的地势与地貌形态逐步被填平。地震层序单元4(SU4)中的沉积中心数量和沉积物厚度相比之前的地震层序单元明显减少,且未发育出明显的背斜或向斜式地貌单元(图16d)。地震层序单元5(SU5)和地震层序单元6(SU6)中发育泥质浊流冲蚀形成的凹坑(图16a),这表明在SU5和SU6中,泥质浊流和海底悬浮沉降的沉

积过程开始占据主导地位。这一现象反映了陆源沉积物输入的减少,且滑坡地貌对沉积厚度的控制已失效。由该沉积盆地的演化历史可知,在空间尺度上,海底滑坡顶界面的负向空间决定着后续砂质浊流沉积的沉积中心的位置和厚度;在时间尺度上,海底滑坡顶界面形态与后续充填的沉积物厚度调控着海底坡度由陡变缓的变化,进而影响了沉积盆地在不同时期的主要沉积动力过程,在盆地由陆源富砂相沉积向深海富泥相沉积的演化过程中发挥了重要作用,对形成良好的油气圈闭和碳封存场所有着积极影响。

3 结论

海底滑坡顶界面形成的复杂海底地形地貌影响了后续浊流的搬运模式,对海洋源汇体系、深海沉积盆地的充填演化历史、海洋矿产资源勘探开发具有重要意义。根据发育位置、规模、形态、成因等因素,海底滑坡顶界面地貌形态可被分为头部排空区、内部断层体系伴生局部负向空间、内部变形块体伴生局部负向空间三种类型,并且不同类型的顶界面负向空间对后续浊流的影响机制不同。首先,海底滑坡头部排空区可作为汇集浊流的优势区,促进大型海底水道或海底峡谷的发育,并为浊流搬运的粗粒碎屑沉积物提供潜在的储集空间。其次,海底滑坡头部正断层体系伴生的顶界面地形地貌通过提供连续的局部地势差来增加浊流的动能和侵蚀能力,为后续浊流体系长距离搬运提供动力。再次,海底滑坡内部块体伴生的顶界面局部地形高点和负向空间通过地形限制了后续浊流水道的搬运路径和决口位置。最后,从沉积盆地尺度而言,海底滑坡顶界面在斜坡建造的大型可容空间不仅可以调控浊流沉积的类型,还可以长时间控制盆地沉积中心的分布和展布范围。通过对海底滑坡顶界面伴生地貌形态的分类及其后续浊流体系影响机制的探讨,海底滑坡顶界面及伴生多尺度负向空间可以有效增强陆缘“源—汇”系统的搬运效率,提升砂质浊流沉积在沉积盆地中的分布范围。对海底滑坡不同顶界面地貌形态进行精细研究可以更好地了解宏观尺度的沉积盆地充填演化历史,也可为后续陆缘碳封存选址和油气藏勘探提供重要地质信息。

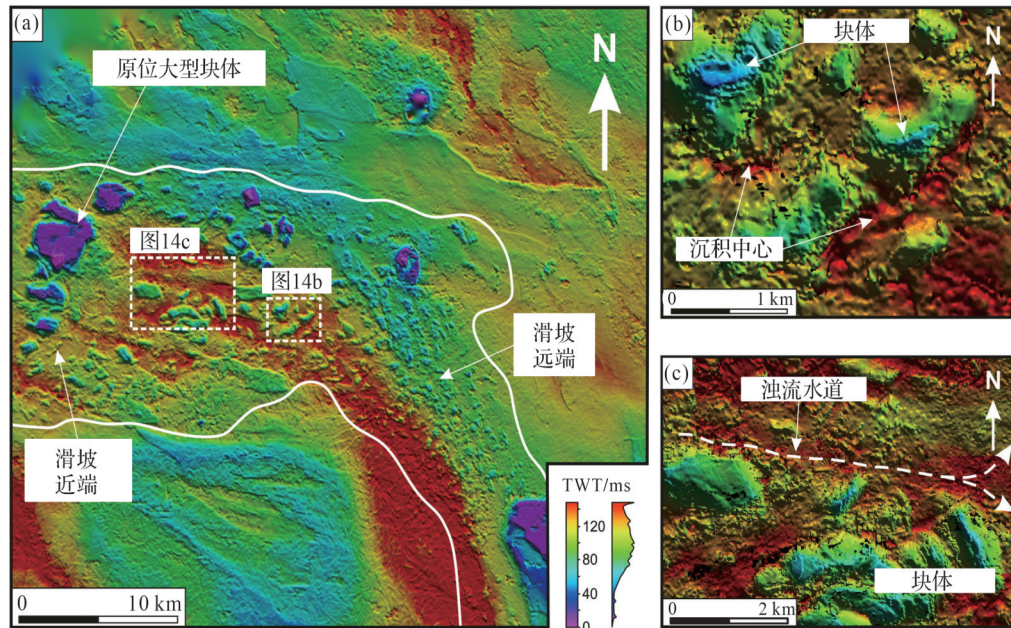


图 14 (a)巴西东南部 Espirito Santo 盆地海底滑坡顶界面地形地貌图; (b)海底滑坡内部块体伴生的相对孤立的顶界面负向空间可作为后续浊流的沉积中心; (c)海底滑坡内部块体伴生的连通性好的顶界面负向空间可作为后续浊流的优先通道(据 Ward *et al.*, 2018 修改)

Fig.14 (a) Topographic map of submarine landslide top surface in Espirito Santo Basin, southeast Brazil; (b) the relatively isolated negative accommodation of the top surface associated with the blocks in the submarine landslide can be used as the depositional centers of subsequent turbidity currents; (c) the well-connected negative accommodation of the top surface associated with the internal blocks of submarine landslides can be used as preferential channel for subsequent turbidity currents (modified from Ward *et al.*, 2018)

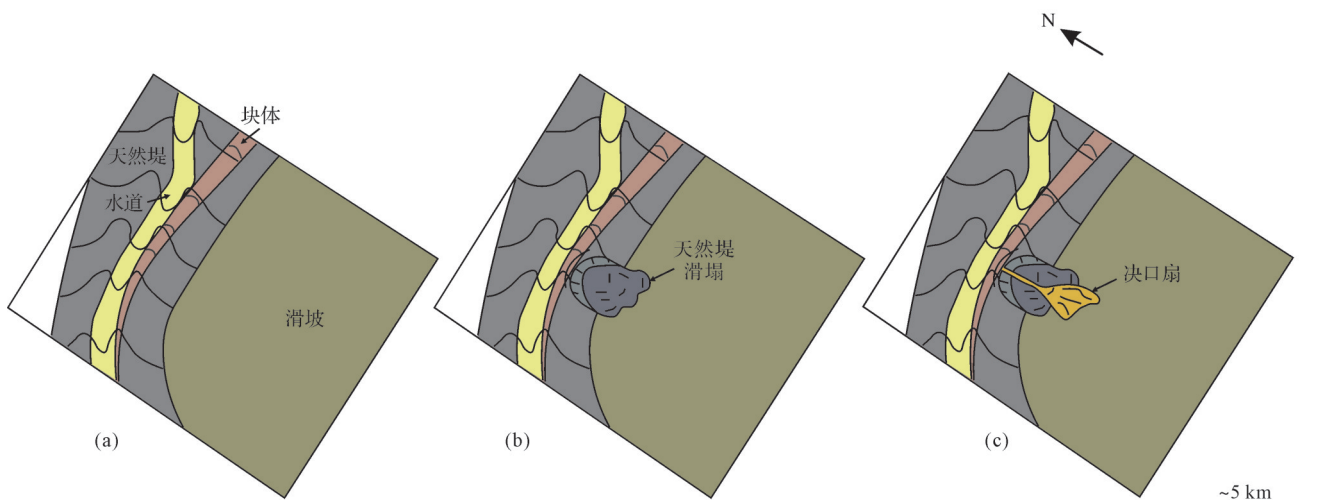


图 15 哥伦比亚北部加勒比海 Magdalena 海底扇浊流水道体系与海底滑坡块体相互作用模式图 (据 Ortiz-Karpf *et al.*, 2015 修改)

(a)海底滑坡块体在顶界面形成地形高点和伴生的负向空间; (b)富泥质的天然堤沉积沿块体侧缘发生滑塌, 浊流水道发生决口; (c)富砂质浊流沉积沿决口进入天然堤滑塌形成的负向空间形成决口扇

Fig.15 Model of interaction between turbidity channel and submarine landslide block in the Magdalena fan of the Caribbean Sea, northern Colombia (modified from Ortiz-Karpf *et al.*, 2015)

(a) bathymetric protrusions and the associated negative accommodations are formed on the top surface by blocks; (b) mud-rich levee deposits collapse along the sharp side edge of the block, and form channel avulsion; (c) sand-rich turbidity sediment enter the negative accommodation formed by the collapsed levee and form the avulsion lobe

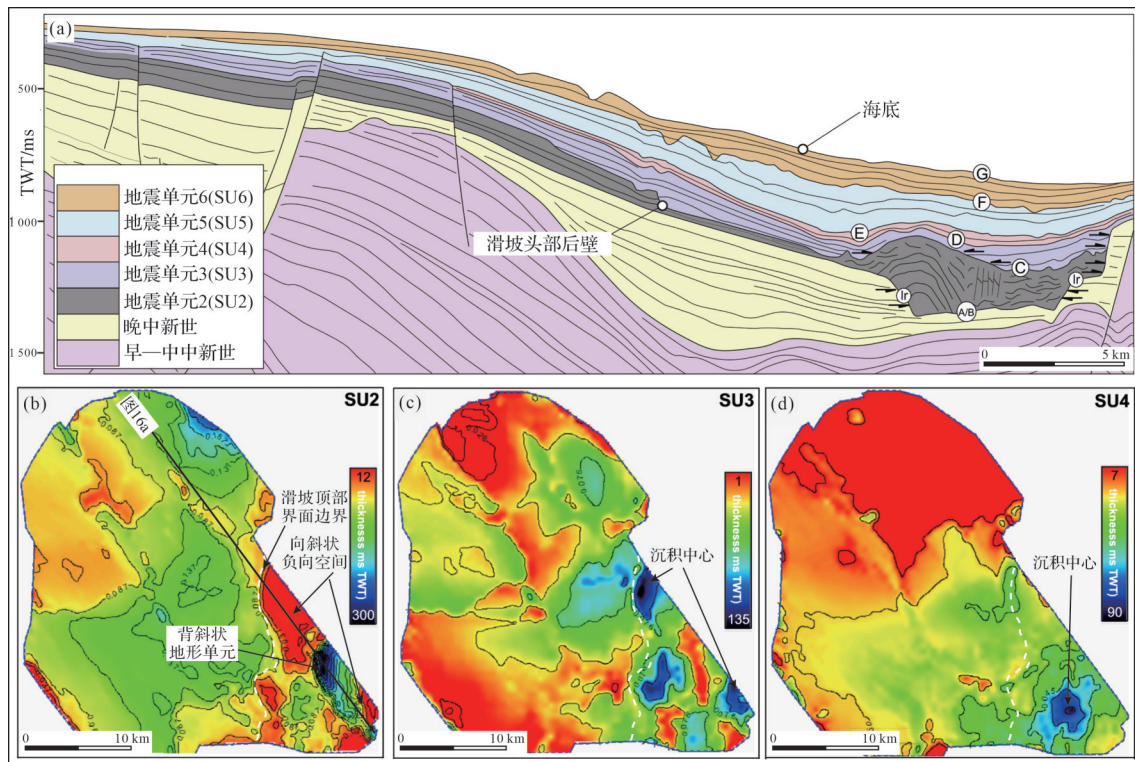


图 16 (a)安哥拉陆缘下刚果盆地上陆坡地震地层格架;(b)SU2 沉积厚度图,海底滑坡断层体系和巨型块体在顶界面伴生大型负向空间(图中东部红色区域);(c)SU3 沉积厚度图,发育一系列近环形的沉积中心(图中东部蓝色区域);(d)SU4 沉积厚度图,沉积中心数量和面积缩小(图中东南部蓝色区域)(据 Olafiranye *et al.*, 2013 修改)

Fig.16 (a) Seismic stratigraphic framework of upper slope of Lower Congo Basin, offshore Angola; (b) SU2 sedimentary thickness map, showing a large negative accommodation (red region in the eastern of figure) on the top surface of the submarine landslide fault system and megaclasts; (b) SU3 sedimentary thickness map with a series of subcircular depositional centers (blue region in the eastern of the figure); (c) SU4 sedimentary thickness map, reduction in the number and area of sedimentary centers (blue region in the southeast of the figure) (modified from Olafiranye *et al.*, 2013)

参考文献 (References)

- 陈珊珊,孙运宝,吴时国. 2012. 南海北部神狐海域海底滑坡在地震剖面上的识别及形成机制[J]. 海洋地质前沿, 28(6): 40-45. [Chen Shanshan, Sun Yunbao, Wu Shiguo. 2012. Sea bottom landslide in the Shenhu area on the north margin of South China Sea and triggering mechanisms[J]. Marine Geology Frontiers, 28(6): 40-45.]
- 丛富云,徐尚. 2017. 陆架边缘迁移轨迹研究现状及应用前景[J]. 地球科学进展, 32(9): 937-948. [Cong Fuyun, Xu Shang. 2017. Research status and application prospect of shelf-edge trajectory analysis[J]. Advances in Earth Science, 32(9): 937-948.]
- 何叶,钟广法. 2015. 海底滑坡及其反射地震识别综述[J]. 海洋科学, 39(1): 116-125. [He Ye, Zhong Guangfa. 2015. Current status of submarine landslides and their seismic recognition[J]. Marine Sciences, 39(1): 116-125.]
- 李伟. 2013. 南海北部海底滑坡的地震特征及成因分析[D]. 青岛:中国科学院研究生院(海洋研究所). [Li Wei. 2013. Seismic characteristics and trigger mechanisms of submarine landslides in northern South China Sea[D]. Qingdao: Institute of Oceanology, Chinese Academy of Sciences.]
- 潘晓仪,李琳琳,王大伟,等. 2023. 南海典型海底滑坡的触发机制及其潜在海啸灾害评估[J]. 地球科学进展, 38(2): 192-211. [Pan Xiaoyi, Li Linlin, Wang Dawei, et al. 2023. Triggering mechanism and tsunamigenic potential of typical submarine landslides in South China Sea[J]. Advances in Earth Science, 38(2): 192-211.]
- 任金锋,孙鸣,韩冰. 2021. 南海南沙海槽大型海底滑坡的发育特征及成因机制[J]. 地球科学, 46(3): 1058-1071. [Ren Jinfeng, Sun Ming, Han Bing. 2021. A giant submarine landslide and its triggering mechanisms on the Nansha trough margin, South China Sea[J]. Earth Science, 46(3): 1058-1071.]
- 孙启良,解习农,吴时国. 2021. 南海北部海底滑坡的特征、灾害评估和研究展望[J]. 地学前缘, 28(2): 258-270. [Sun Qiliang, Xie Xinong, Wu Shiguo. 2021. Submarine landslides in the northern South China Sea: Characteristics, geohazard evaluation and perspectives[J]. Earth Science Frontiers, 28(2): 258-270.]
- 孙运宝,吴时国,王志君,等. 2008. 南海北部白云大型海底滑坡的几何形态与变形特征[J]. 海洋地质与第四纪地质, 28(6): 69-77.

- [Sun Yunbao, Wu Shiguo, Wang Zhijun, et al. 2008. The geometry and deformation characteristics of Baiyun submarine landslide [J]. *Marine Geology & Quaternary Geology*, 28(6): 69-77.]
- 王大伟, 吴时国, 吕福亮, 等. 2011. 南海深水块体搬运沉积体系及其油气勘探意义[J]. *中国石油大学学报(自然科学版)*, 35(5): 14-19. [Wang Dawei, Wu Shiguo, Lü Fuliang, et al. 2011. Mass transport deposits and its significance for oil & gas exploration in deep-water regions of South China Sea[J]. *Journal of China University of Petroleum*, 35(5): 14-19.]
- 王大伟, 吴时国, 秦志亮, 等. 2009. 南海陆坡大型块体搬运体系的结构与识别特征[J]. *海洋地质与第四纪地质*, 29(5): 65-72. [Wang Dawei, Wu Shiguo, Qin Zhiliang, et al. 2009. Architecture and identification of large Quaternary mass transport depositions in the slope of South China Sea[J]. *Marine Geology & Quaternary Geology*, 29(5): 65-72.]
- 吴时国, 秦蕴珊. 2009. 南海北部陆坡深水沉积体系研究[J]. *沉积学报*, 27(5): 922-930. [Wu Shiguo, Qin Yunshan. 2009. The research of deepwater depositional system in the northern South China Sea[J]. *Acta Sedimentologica Sinica*, 27(5): 922-930.]
- Abu C, Jackson C A L, Francis M. 2022. Strike-slip overprinting of initial co-axial shortening within the toe region of a submarine landslide and a model for basal shear surface growth: A case study from the Angoche Basin, offshore Mozambique[J]. *Journal of the Geological Society*, 179(2): jgs2021-2032.
- Alves T. 2015. Submarine slide blocks and associated soft-sediment deformation in deep-water basins: A review[J]. *Marine and Petroleum Geology*, 67: 262-285.
- Amaechi P O, Waldmann N D, Makovsky Y, et al. 2023. Characterization of blocks within a near seafloor Neogene MTC, Orange Basin: Constraints from a high-resolution 3D seismic data[J]. *Sedimentary Geology*, 444: 106319.
- Armitage D A, Romans B W, Covault J A, et al. 2009. The influence of mass-transport-deposit surface topography on the evolution of turbidite architecture: The Sierra Contreras, Tres Pasos Formation (Cretaceous), southern Chile[J]. *Journal of Sedimentary Research*, 79(5): 287-301.
- Bondevik S, Løvholt F, Harbitz C, et al. 2005. The Storegga Slide tsunami—comparing field observations with numerical simulations [J]. *Marine and Petroleum Geology*, 22(1/2): 195-208.
- Bull S, Browne G, Arnot M J, et al. 2020. Influence of mass transport deposit (MTD) surface topography on deep-water deposition: An example from a predominantly fine-grained continental margin, New Zealand[J]. *Special Publications*, 500(1): 147-171.
- Bull S, Cartwright J, Huuse M. 2009. A review of kinematic indicators from mass-transport complexes using 3D seismic data[J]. *Marine and Petroleum Geology*, 26(7): 1132-1151.
- Buso V V, Kneller B, Assis V d S R, et al. 2024. Incorporation of substrate blocks into mass transport deposits: Insights from subsurface and outcrop studies[J]. *The Depositional Record*, 10(5): 708-719.
- Collot J Y, Lewis K, Lamarche G, et al. 2001. The giant Ruatoria debris avalanche on the northern Hikurangi margin, New Zealand: Result of oblique seamount subduction[J]. *Journal of Geophysical Research: Solid Earth*, 106(B9): 19271-19297.
- Frey-Martínez J, Cartwright J, James D. 2006. Frontally confined versus frontally emergent submarine landslides: A 3D seismic characterisation[J]. *Marine and Petroleum Geology*, 23(5): 585-604.
- Gee M, Uy H, Warren J, et al. 2007. The Brunei slide: A giant submarine landslide on the north west Borneo margin revealed by 3D seismic data[J]. *Marine Geology*, 246(1): 9-23.
- Georgiopoulou A, Masson D G, Wynn R B, et al. 2010. Sahara Slide: Age, initiation, and processes of a giant submarine slide[J]. *Geochimistry, Geophysics, Geosystems*, 11(7): Q07014.
- Hafliðason H, Lien R, Sejrup H P, et al. 2005. The dating and morphometry of the Storegga Slide[J]. *Marine and Petroleum Geology*, 22(1/2): 123-136.
- Henriksen S, Helland-Hansen W, Bullimore S. 2011. Relationships between shelf-edge trajectories and sediment dispersal along depositional dip and strike: a different approach to sequence stratigraphy [J]. *Basin Research*, 23(1): 3-21.
- Kneller B, Dykstra M, Fairweather L, et al. 2016. Mass-transport and slope accommodation: Implications for turbidite sandstone reservoirs[J]. *AAPG Bulletin*, 100(2): 213-235.
- Li W, Alves T M, Urlaub M, et al. 2017. Morphology, age and sediment dynamics of the upper headwall of the Sahara Slide Complex, Northwest Africa: Evidence for a large Late Holocene failure[J]. *Marine Geology*, 393: 109-123.
- Li W, Wu S, Völker D, et al. 2014. Morphology, seismic characterization and sediment dynamics of the Baiyun Slide Complex on the northern South China Sea margin[J]. *Journal of the Geological Society*, 171(6): 865-877.
- Martinsen O J, Bakken B. 1990. Extensional and compressional zones in slumps and slides in the Namurian of county Clare, Ireland[J]. *Journal of the Geological Society*, 147(1): 153-164.
- Micallef A, Masson D G, Berndt C, et al. 2016. Submarine spreading in the Storegga slide, Norwegian Sea[J]. *Memoirs*, 46(1): 411-412.
- Moernaut J, De Batist M. 2011. Frontal emplacement and mobility of sublacustrine landslides: Results from morphometric and seismic stratigraphic analysis[J]. *Marine Geology*, 285(1/2/3/4): 29-45.
- Moore G F, Gamboa D, Barnes P, et al. 2023. High quality seismic images confirm Ruatoria Mass Transport Deposit at IODP Site U1520, northern Hikurangi subduction zone[C]. AGU Fall meeting. San Francisco: AGU, 1322: OS13D-1322.
- Moscardelli L, Wood L, Mann P. 2006. Mass-transport complexes and associated processes in the offshore area of Trinidad and Venezuela [J]. *AAPG Bulletin*, 90(7): 1059-1088.
- Moscardelli L, Wood L. 2008. New classification system for mass transport complexes in offshore Trinidad[J]. *Basin Research*, 20(1): 73-98.
- Nardin T R, Hein F, Gorsline D S, et al. 1979. A review of mass movement processes, sediment and acoustic characteristics, and contrasts

- in slope and base-of-slope systems versus canyon-fan-basin floor systems[M]. Tulsa: SEPM Special Publication, 27: 61-73.
- Nemec W. 1990. Aspects of sediment movement on steep delta slopes [J]. *Coarse-grained deltas*, 10(2): 29-73.
- Nugraha H D, Jackson C, Johnson H, et al. 2020a. Evolution of flow cells within a mass-transport complex: Insights from the Gorgon Slide, offshore NW Australia (preprint) [J/OL]. *EarthArXiv*: 1-49. [2020-03-25].
- Nugraha H D, Jackson C A L, Johnson H D, et al. 2020b. Lateral variability in strain along a mass-transport complex (MTC) toewall:[J]. *Journal of the Geological Society*, 177(6): 1261-1279.
- Nugraha H D, Jackson C A L, Johnson H D, et al. 2022. Extreme erosion by submarine slides[J]. *Geology*, 50(10): 1130-1134.
- Nwoko J, Kane I, Huuse M. 2020. Mass transport deposit (MTD) relief as a control on post-MTD sedimentation: Insights from the Taranaki Basin, offshore New Zealand[J]. *Marine and Petroleum Geology*, 120: 104489.
- Olafiranye K, Jackson C A L, Hodgson D M. 2013. The role of tectonics and mass-transport complex emplacement on upper slope stratigraphic evolution: A 3D seismic case study from offshore Angola [J]. *Marine and Petroleum Geology*, 44: 196-216.
- Ortiz-Karpf A, Hodgson D M, Jackson C A L, et al. 2018. Mass-transport complexes as markers of deep-water fold-and-thrust belt evolution: insights from the southern Magdalena fan, offshore Colombia[J]. *Basin Research*, 30(S1): 65-88.
- Ortiz-Karpf A, Hodgson D M, McCaffrey W. 2015. The role of mass-transport complexes in controlling channel avulsion and the subsequent sediment dispersal patterns on an active margin: The Magdalena fan, offshore Colombia[J]. *Marine and Petroleum Geology*, 64: 58-75.
- Qin Y, Alves T, Constantine J, et al. 2017. The role of mass wasting in the progressive development of submarine channels (Espírito Santo Basin, Se Brazil) [J]. *Journal of Sedimentary Research*, 87(5): 500-516.
- Sawyer D, Flemings P, Dugan B, et al. 2009. Retrogressive failures recorded in mass transport deposits in the Ursa Basin, northern gulf of Mexico[J]. *Journal of Geophysical Research*, 114(B10): B10102.
- Scarselli N, McClay K, Elders C. 2013. Submarine slide and slump complexes, Exmouth Plateau, NW Shelf of Australia[M]. Perth: The sedimentary basins of western Australia IV: Proceedings of the petroleum exploration society of Australia symposium: 1-20.
- Stagna M D, Maselli V, van Vliet A. 2023. Large-scale submarine landslide drives long-lasting regime shift in slope sediment deposition [J]. *Geology*, 51(2): 167-173.
- Steventon M, Jackson C, Hodgson D, et al. 2019. Strain analysis of a seismically imaged mass-transport complex, offshore Uruguay[J]. *Basin Research*, 31(3): 600-620.
- Sun Q, Alves T M, Lu X, et al. 2018a. True volumes of slope failure estimated from a Quaternary mass-transport deposit in the northern South China Sea[J]. *Geophysical Research Letters*, 45(6): 2642-2651.
- Sun Q, Cartwright J, Xie X, et al. 2018b. Reconstruction of repeated Quaternary slope failures in the northern South China Sea[J]. *Marine Geology*, 401: 17-35.
- Ward N, Alves T M, Blenkinsop T, et al. 2018b. Submarine sediment routing over a blocky mass-transport deposit in the Espírito Santo Basin, SE Brazil[J]. *Basin Research*, 30(4): 816-834.
- Williams S C P. 2016. Skimming the surface of underwater landslides [J]. *Proceedings of the National Academy of Sciences*, 113(7): 1675-1678.
- Wu N, Nugraha H D, Zhong G, et al. 2022. The role of mass-transport complexes in the initiation and evolution of submarine canyons[J]. *Sedimentology*, 69(5): 2181-2202.
- Wu N, Zhong G, Niyazi Y, et al. 2024. Transformation of dense shelf water cascade into turbidity currents: Insights from high-resolution geophysical datasets[J]. *Earth and Planetary Science Letters*, 626: 118547.

Top Surface Geomorphology of Submarine Landslides and Its Impact on Turbidity Currents

LI WenJing¹, WU Nan¹, KUANG ZengGui², REN JinFeng², WANG BiWen¹, HAN ZhengHao¹,
CHEN WanLi³

1. State Key Laboratory of Marine Geology, Tongji University, Shanghai 200092, China

2. Guangzhou Marine Geological Survey, Guangzhou 510075, China

3. Institute of Deep-sea Science and Engineering, Chinese Academy of Sciences, Sanya, Hainan 572000, China

Abstract: [Objective] The catastrophic failure of large submarine landslides can result in the deformation and destruction of thousands of square kilometers of seafloor, transporting hundreds to thousands of cubic kilometers of submarine sediments. This process dramatically reconstructs the seafloor topography of the continental shelf-slope region and has a profound impact on subsequent submarine sedimentation processes. [Methods] The topographic features of different large submarine landslides were qualitatively described using multibeam bathymetric and seismic reflection data, and the key geometric parameters of the submarine landslide top surface, such as area and volume, were quantitatively characterized. Based on the scale, morphological features, and formation mechanisms of the associated reliefs on the submarine landslide top surface, these landslides were separated into three categories: head evacuation zone, locally negative accommodation associated with internal fault systems, and locally negative accommodation associated with internal deformation blocks. The mechanisms of the three types of negative accommodation on the subsequent turbidity current system are then discussed separately. [Results] Firstly, the head evacuation zone is typically associated with hundreds to thousands of square kilometers of negative accommodation, which acts as a "funnel" during sediment transport along the continental margin, effectively capturing and concentrating subsequent turbidity currents while enhancing the transport efficiency of gravel and coarse sand and playing a crucial role in the accumulation of marine organic matter. Secondly, the striped negative accommodation associated with internal fault systems and the irregular negative accommodation associated with internal deformation blocks can regulate the sedimentation dynamics of subsequent turbidity currents, such as constraining flow direction, enhancing erosion intensity, and forcing channels to avulse. Finally, the negative accommodations associated with the submarine landslide top surface may produce synergistic effects, influencing the sediment filling and evolution of sedimentary basins and the distribution of sedimentary centers over millions of years. [Conclusions] The investigation of the morphological characteristics of submarine landslide top surfaces and their controlling effects on the subsequent turbidity currents sedimentary dynamic process can provide key geological information for clarifying the transport process of marginal sediments, identifying the distribution of sand-rich reservoirs in deep-sea sedimentary basins, and predicting the development range of catastrophic turbidity currents.

Key words: submarine landslide; landslide top surface geomorphology; submarine turbidity current